PANORAMIC CRYSTALLOGRAPHIC ANALYSIS OF STRUCTURE EVOLUTION IN LOW-CARBON MARTENSITIC STEEL UNDER TEMPERING

A. A. Zisman,[1, 2] N. Yu. Zolotorevsky,[2] S. N. Petrov,[1, 2] E. I. Khlusova,[1, 2] and E. A. Yashina[1]

Structural changes developing under tempering of low-carbon martensitic steel are studied by the method of electron backscatter diffraction. The evolution of the crystal lattice curvature reflecting the softening process and the packet-block structure of the martensite are analyzed. The dependence of the self-accommodation of packets on the combination of variants of the interphase orientation relation is determined. The growth of new martensite laths under tempering, which is related to this dependence, is considered.

Key words: low-carbon steel, martensite, phase stresses, tempering, lattice curvature, orientation relation.

INTRODUCTION

Quantitative analysis of changes in the structural state of steels during tempering remains an urgent problem. On the one hand, optical microscopy does not allow us to detect decrease in the dislocation density and commonly has insufficient resolving power for analysis of the evolution of carbide phases. On the other hand, the methods of transmission electron microscopy (TEM) efficient for the micron and submicron scales are poorly suitable for certifying the structure in statistically representative regions of a material. The best compromise between the limitations mentioned is panoramic imaging of crystal lattice orientations with the help of electron backscatter diffraction (EBSD). This method combined with scanning electron microscopy (SEM) [1] requires conventional metallographic specimens where local orientations are measured accurate to tenths of a degree at the cites of a virtual mesh with a step of about 0.1 μm. The accuracy of EBSD analysis may be raised additionally by prolonging the exposition of each cite [2]. However, when the time of the scanning is limited, this requires reduction of the sizes (the representativeness) of the regions studied or enlargement of the distances between the measured points, i.e., lowering of the resolving power of the method.

In addition to local lattice orientations, processing of primary data of EBSD makes it possible to determine the corresponding curvature (orientation gradient) [3], which is related directly to lattice defects. Thus, it is possible to map the inhomogeneity of the dislocation density in the analyzed regions without detecting individual dislocations. Specifically, this approach makes it possible to detect "smeared" dislocation boundaries with very low (about 0.5°) misorientation angles [4] and the distribution of the plastic strain and of the sources of recrystallization inside grains [5, 6]. In the latter case we may use standard options of the EBSD software [7], such as KAM (kernel average misorientation) and GAM (grain average misorientation). Similar techniques are used to identify and map the varieties of α-phase (ferrite, bainite, martensite) [8, 9], which differ from each other in the dislocation density by an order of magnitude, but are by far not always determinable with the help of optical microscopy where their morphological features are concerned. However, in the case of tempering such an analysis is complicate in principle, because the rate of the softening of different structural components is not the same; in particular, martensite becomes closer to bainite with respect to the dislocation density. Moreover, in addition to the dislocation structure, the elastic distortions of the lattice are affected by the shape of the interacting crystals; they may be indistinguishable with respect to the curvature even at different dislocation densities [9]. With allowance for these difficulties, it is expedient to characterize the structural state of a steel changing during tempering by the integral spectrum of the curvature. In addition to the general softening, which manifests itself in the decrease of the respective mean value, the gradual variation of the form (for example, the splitting) of the spectrum reflects

---

[1] Central Research Institute of Structural Materials 'Prometey,' St. Petersburg, Russia (e-mail: npk3@crism.ru).
[2] Peter the Great St. Petersburg Polytechnic University, St. Petersburg, Russia.

the specific kinetics of tempering of different structural components of the α-phase. In the present study, this approach is applied to a low-carbon martensitic steel containing a small fraction of bainite. We compare the curvature spectra plotted from the EBSD data in quenched condition and after different variants of tempering of the steel.

In addition to the high dislocation density and the corresponding curvature of the lattice, martensitic and bainitic structures are characterized by a manifested orientation relation (OR), i.e., a specific set of variants V_i (i = 1, 2, ..., 24) for the orientation of transformed crystals with respect to the original austenite. Though the OR itself remains virtually invariable for a specific steel, the distribution of laths or blocks in its variants determined with the help of EBSD in terms of the probability of their conjugation (V_i/V_j, $i \neq j$) on the interfaces is extremely sensitive to their structural state [10 – 13]. Specifically, the martensitic component of the α-phase differs noticeably from the bainitic component with respect to this feature. The varieties of bainite differ from each other depending on the temperature of their formation. However, as far as we know, analysis of the "selection of variants" has not been applied in the studies of the structural evolution of martensite under tempering, despite the following prerequisites:

(*1*) migration mobility of large-angle boundaries (LAB) in high tempering of low-carbon martensite [14];

(*2*) existence of the driving force for variation of the lath structure, because the shear deformation of each packet and the elastic distortions due to its constraint by the surrounding material depend on the volume fraction of laths belonging to different variants of OR.

We used the representative data of the EBSD to determine the interphase OR of the studied steel and the statistics of conjugation of its variants in quenched condition and after different variants of tempering. The thus determined changes in the structure of the martensite were then proved by mapping of individual variants of OR at a local level.

The aim of the present work was to use the possibilities of quantitative EBSD analysis for studying the evolution of the structure of high-strength steels during tempering. The choice of a low-carbon high-strength steel for the study was determined by its martensitic structure, where the effects of high tempering were well manifested.

METHODS OF STUDY

We studied commercial rolled low-carbon (0.09% C) martensitic steel 09KhN4MDF in quenched condition and after tempering at 625°C for 8 h and at 660°C for 1 and 6 h. Laps with the plane perpendicular to the rolling direction were prepared from specimens cut from the middle (over the thickness) part of a sheet. We resorted to usual metallographic procedures. To remove the surface mechanical hardening in the final stage, we used a special paste based on colloidal alumina. We performed a panoramic EBSD analysis of the laps with the help of a Quanta 200 3D FEG scanning electron microscope (SEM) with scanning step $d = 0.1$ μm; to determine the local orientations from the diffraction data, we used the EDAX TSL software. The conventional "metallographic" structures were maps of the EBSD data in gray color tints obtained with the help of a standard image quality (IQ) option, which detects the boundaries and other defects from contrast of the diffraction lines. The thus plotted two-dimensional maps virtually do not differ from the images obtained by optimum modes of optical microscopy after polishing and chemical etching of laps.

We evaluated the lattice curvatures of whole crystals (laths or blocks) of transformed structure with the help of the GAM function, which is a standard option of the TSL OIM Analysis software. This function characterizes the mean value of the angle of turn of the lattice between adjacent points of measurement within a region separated from the surrounding by a boundary with misorientation angle no smaller than the specified tolerance angle θ_t. In the present work we used $\theta_t = 5°$, which is close in steels to the angle of relative turn between the possible variants of the OR of the α-phase with a common lattice of the original austenite [10, 11]. This eliminates the contribution of interfaces of different martensite or bainite crystals into the determined value of GAM, i.e., reflects only their own curvature. In addition, each crystal is indeed characterized as a whole one, because the low-angle boundaries ($\theta < \theta_t$) inside it are not isolated.

The curvature associated with the lattice defects and mapped as an orientation gradient [3, 4] was estimated in terms of the ratio of the GAM (in degrees), i.e., the averaged measure of the turn of the lattice between adjacent EBSD points, to the distance d [μm] between them. Though at the specified d this estimate is proportional to the GAM and preserves the kind of the distribution of this parameter in the analyzed range, such a seemingly formal normalization has a principal sense, because it renders the curvature K a regular physically dimensional quantity [°/μm] and, accordingly, indicates that the mapping of the structure may possibly be dependent on d. The causes of such a dependence and the corresponding methodological constraints will be considered in the discussion of the results of our study. However, we may say in advance that the spectra of the distribution of the curvature obtained by us at $d = 0.1$ μm have turned out to be quite sensitive to the tempering conditions.

The interphase OR determined by the chemical composition of the steel and by the conditions of the martensitic transformation commonly deviate from each other and from the canonical Kurdyumov–Sachs or Nishiyama relations by several degrees [10, 11]. Therefore, it is necessary to know the specific OR present in the transformed structure for its accurate crystallographic analysis. We determined the OR from the EBSD structure by the method of [12], which is based on statistical analysis of the misorientations on interfaces in the α-phase and does not require detection of the for-
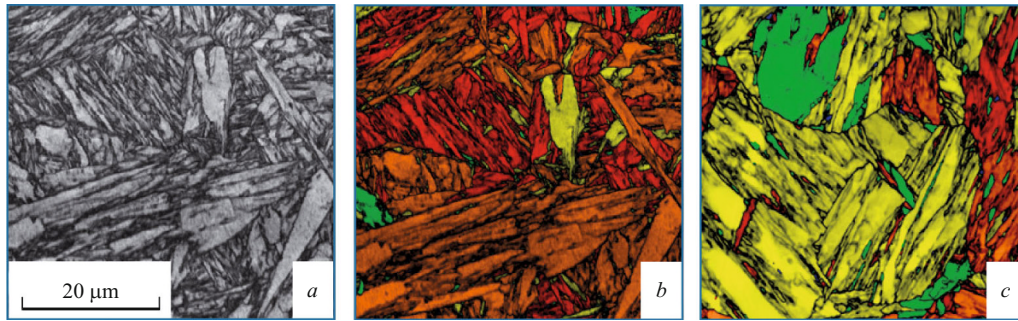
Fig. 1. EBSD mapping of the structure of steel 09KhN4MDF after quenching (*a, b*) and after quenching and tempering at 625°C (*c*) with the help of the "Image Quality" function (*a*) and its imposition onto lattice curvature maps (*b, c*; the color palette is deciphered in Table 1).

mer austenite grains. Then, the vectors θ_{ij} of relative turn between various variants of the determined OR ($i, j = 1, 2, ..., 24; i \neq j$) were compared to the actual misoreintations θ between crystals of the α-phase. This gave us regions of boundaries ($|\theta| > \theta_t$), where the angular deviation of the misorientation of some θ_{ij} did not exceed 1°. With such a sample, the orientation on one side of each boundary was put into correspondence to the first variant of the OR (V_1) and the variant of the OR (one from the set $V_2 - V_{24}$) on the other side of the boundary was numbered as a function of θ in accordance with the chosen classification [10, 11]. The relative lengths of the thus singled out boundaries with various combinations of variants of the OR (V_1/V_2, V_1/V_3, ..., V_1/V_{24}) were used to plot the corresponding spectra for the studied steel after quenching and after different variants of tempering. Such spectra, which make it possible to recognize objectively the structural varieties of bainite and martensite [10, 11] in quenched steels, were applied to post-tempering structures for the first time. To take into account the possible changes in the crystallography of martensite as a result of growth of relatively thin laths, we studied the dependence of the spectra obtained on the EBSD scanning step, which was varied within $0.1 - 0.8$ µm by successive elimination of a part of the discrete data (points of the initial mesh). In addition, to determine the growing crystals, the corresponding OR variants were mapped individually against the background of the transformed structure.

TABLE 1. Color Mapping of the Crystal Lattice Curvature of Steel 09KhN4MDF

Color	Curvature range, °/µm	Structural varieties of α-phase [12]
Blue	0 – 4.0	Ferrite
Green	4.0 – 5.5	Ferrite + bainite
Yellow	5.5 – 7.0	Bainite
Orange	7.0 – 8.5	Bainite +
Red	> 8.5	martensite

RESULTS AND DISCUSSION

The structure of quenched steel 09KhN4MDF mapped in accordance with the EBSD analysis with the help of the IQ function is presented in Fig. 1*a*; the imposed map of the crystal curvature (the ratio of the GAM to the EBSD scanning step) is presented in Fig. 1*b*. To map the curvature, we used the tabulated color palette together with the preliminary data of [12] on its interrelation with different components of the α-phase after quenching. These data and the typical structural features (Fig. 1*a*) reflect dominant fraction of the martensite component. Tempering of the steel quenched from 625°C does not introduce noticeable changes into the "metallographic" mapping of the structure with the help of the IQ function, which is not presented individually. However, the level of the curvature (Fig. 1*c*) lowers considerably, and the tempered martensite can hardly be distinguished from bainite in quenched condition with respect to this feature.

Evolution of the Curvature Spectrum

To make a more detailed analysis of the results obtained we should take into account that the structural components of the α-phase differing in the density of the lattice dislocations and, accordingly, in the values of the elastic distortions of the crystal, change their state differently in the process of tempering. This is easily detectable when we compare the spectra of their distribution with respect to the curvature level K [°/µm] (Fig. 2*a*). As could be expected, the quenched condition is characterized by a bimodal spectrum with a principal martensitic peak and a relatively weak maximum due to the low (up to 10%) fraction of bainite.

The tempering produces not only the expected general decrease in the curvature but also a substantial change in the shape of the spectrum in accordance with scheme presented in Fig. 2*b*. If we neglect the weaker features of Fig. 2*a*, the martensite peak (in contrast to the bainite one) splits due to the slower shifting of its right-hand part M_2 matching the highest dislocation density. On the face of it, this may seem strange, because the density of the elastic energy (the driving

force of the structural evolution) is maximum in the corresponding martensite regions. At the same time, such splitting is expectable from the standpoint of the kinetics, because the excess dislocation density hinders rearrangement of the dislocations with progressive annihilation. In addition to the influence of the initial dislocation density in accordance with Fig. 2*b*, this effect may also be connected with the difference in the thickness of the martensite laths, which also affects the evolution of their defect structure under tempering. Though we can hardly predict the result of the competition of all the mentioned factors as a function of the tempering conditions, the example considered demonstrates efficiency of the curvature spectrum as a representative characteristic of the structural state of the α-phase.

The sensitivity of the curvature spectrum to the conditions of heat treatment was studied for specimens of quenched steel 09KhN4MDF subjected to tempering for 1 h or 6 h at a higher temperature of 660°C. The curvature maps and the respective spectra (see Fig. 3) were plotted as in the previous case. After 1-h tempering at 660°C and 8-h tempering at 625°C the right-hand martensitic peaks (M_2^* in Fig. 2*b*) turned out to be similar, whereas the other spectra differed noticeably. Specifically, it should be noted that comparing Fig. 2*a* and Fig. 3*b*, we see that the peaks of the tempered bainite (B^*) and the features of its merging with the left-hand martensite peak (M_1^*) are weakened. When the duration of the tempering at 660°C is increased to 6 h (Fig. 3*d*), this merging finishes, and the right-hand peak of martensite M_2^* becomes a principal one primarily due to partial absorption of the less distorted component M_1^*.

Martensite or bainite structures are detectable reliably, in accordance with [10, 11], from the spectrum of the intervariant orientations after quenching; however, the effectiveness of this approach in the study of tempering kinetics is not obvious. Indeed, there exist an established opinion that tempering causes lowering of the dislocation density and/or redistribution of carbon, but the lath-packet structure of the martensite remains invariable. A known exception [14], which is not considered here, is recrystallization of martensite with extremely low carbon content (< 0.01%) at tempering temperatures close to Ac_1, which transforms the lath structure into a coarse-grained one.

To include the finest structural components into the analyzed statistics of intervariant misorientations we conducted EBSD scanning at a step of 0.1 μm, which is 5 times smaller than that in [10, 11]. The OR determined in accordance with the data of [12] is characterized by the Euler angles (27.89° 8.81° 18.25°) for turning the cubic elementary cells in the γ – α transformation and matches the interphase deviation angles of 1.59° and 2.58° for the close-packed planes and directions, respectively. The frequency spectra of conjugation of the variants of this OR on interfaces after different heat treatments are presented in Fig. 4. Despite the higher spatial resolution, the result obtained for the martensite is
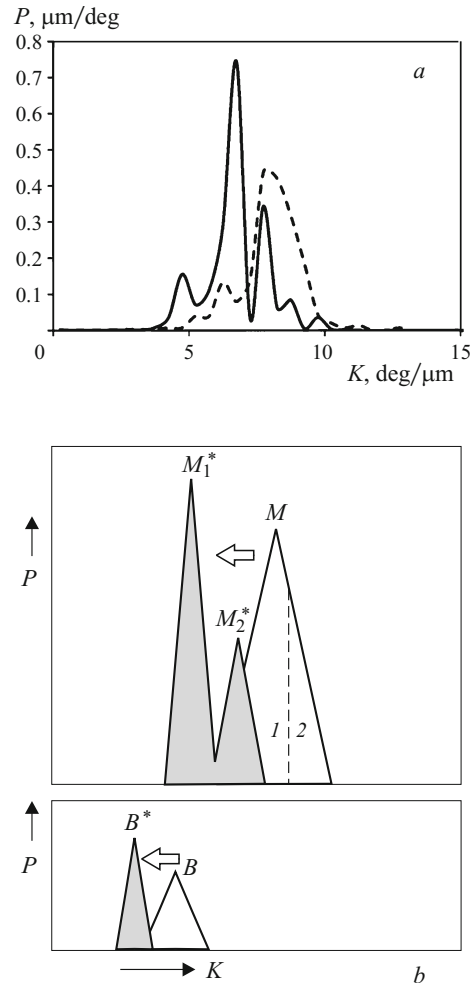
Fig. 2. Spectra of the distribution of curvature K of the crystal lattice of quenched steel 09KhN4MDF prior to and after tempering at 625°C (the dashed and solid lines, respectively) (*a*) and diagram of the evolution of martensite (M) and bainite (B) components of the spectrum (P is the proportion of the area of the lap (structure) per unit range of the curvature).

usual (as in [10, 11]). Tempering causes unexpectedly strong evolution of the spectrum, i.e., growth of some crystals (laths or blocks) of the α-phase at the expense of others. We should mention the growth in the fraction of intervariant misorientation V_2/V_1 and lowering of the fraction of V_4/V_1. The longer tempering at 625°C produces a weaker effect than 1-h tempering at 660°C (Fig. 4*b* and *c*). With growth of the duration of the tempering at 660°C to 6 h (Fig. 4*d*), the spectrum acquires a form close to that of the low-temperature variety of bainite in quenched steel, when the EBSD analysis is conducted with scanning step 0.5 μm [10, 11].

For correct understanding of the results presented we should bear in mind that the fractions P_i of the intervariant misorientations (V_i/V_1, $i = 2, 3, ..., 24$) were determined in terms of the relative lengths of the respective interfaces and not in terms of the volume of the laths V_i. Their sizes in the
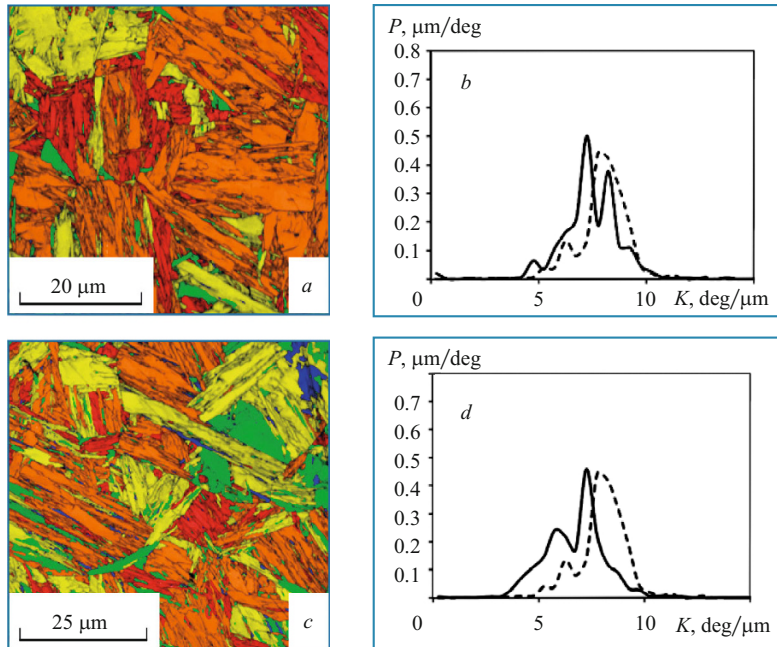
Fig. 3. Maps (*a, c*) and distribution spectra (*b, d*) of the crystal lattice curvature of steel 09KhN4MDF after quenching (the dashed lines) and after quenching and tempering at 660°C (the solid lines): *a, b*) tempering for 1 h; *c, d*) tempering for 6 h.

plane of occurrence exceed the thickness, which affects P_i but weakly, by an order of magnitude. However, if such laths

are too thin with respect to the scanning step d, they will not be allowed for in construction of the spectrum of intervariant misorientations. This is illustrated by the spectra for one of the studied states (after 1-h tempering at 660°C) plotted from the EBSD data with d varied from 0.1 to 0.8 μm (Fig. 5). It can be seen that at $d \geq 0.4$ μm, the effect of the scanning step (the apparent decrease in the fraction of V_2) weakens noticeably, which allows us to make a rough estimate of the mean thickness of the crystals corresponding to variant V_2 of the orientation relation.

Growth of Individual Martensite Laths During Tempering

The determined regular features indicate indirectly that tempering causes growth of martensite crystals with the orientation with respect to the surrounding meeting conjugation V_2/V_1 of the OR variants. To confirm this fact, we used EBSD to find the respective closed regions in quenched condition and after 1-h and 6-h tempering at 660°C. The boundaries of these regions are colored blue in Fig. 6 to distinguish them from all the other (black) boundaries with $\theta > \theta_t = 5°$. The obtained images leave no doubt that individual laths (V_2) inside martensite packets (V_1) do grow in the tempering process virtually
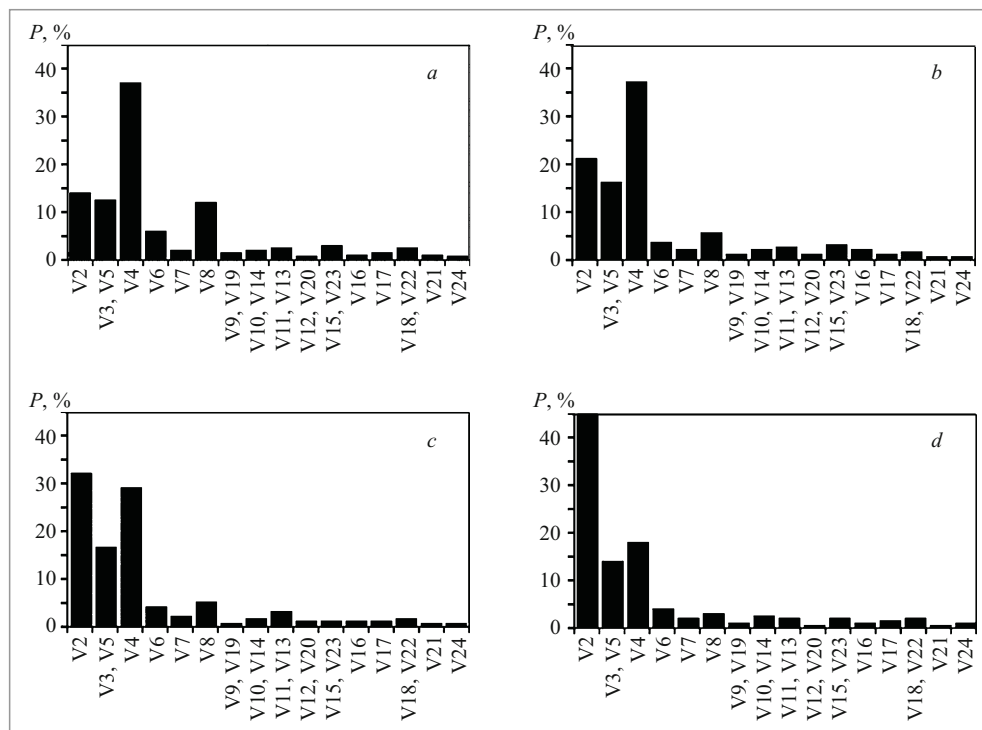
Fig. 4. Spectra of the distribution of variants of misorientation between adjacent crystals of α-phase matching the orientation relation γ/α in steel 09KhN4 MDF: *a*) after quenching; *b*) after quenching and 8-h tempering at 625°C; *c, d*) 1-h and 6-h tempering at 660°C, respectively.
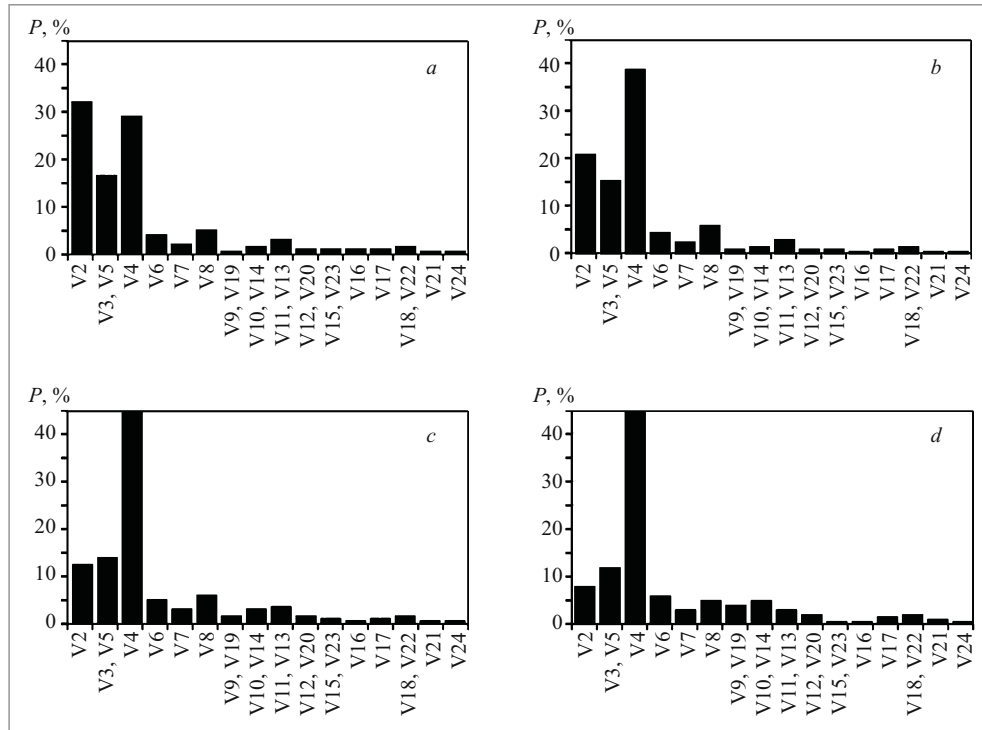
Fig. 5. Spectra of the distribution of variants of misorientation between adjacent crystals of α-phase matching the orientation relation γ/α in steel 09KhN4 MDF after 1-h tempering at 660°C according to the EBSD data at scanning step 0.1 (*a*), 0.2 (*b*), 0.4 (*c*) and 0.8 μm (*d*).

without changing their thickness (about 1 μm). At the same time, the content of the laths mapped in Fig. 6*b* and *c* increases as compared to those in Fig. 6*a*. It seems that some of them have not been detected in the quenched condition at the scanning step of 0.1 μm due to their too small sizes.

DISCUSSION

When mapping the curvature with the help of the GAM function, we should bear in mind that in the general case the results depend on the proportion of the scanning step d to the characteristic scale L of the dislocation structure, within which the orientation of the lattice varies monotonically. At $d \ll L$ the angle of the misorientation between the adjacent analyzed points and its averaged values (GAM) are approximately proportional to d. At the same time, at $d \gg L$ the values of this angle are distributed randomly in the range between zero and maximum, and the averaged parameter GAM becomes virtually independent of d. In the case of a uniform distribution of the lattice dislocations, which are the sources of curvature with density $\rho \sim 10^{10} - 10^{11}$ cm^{-2} typical for bainite-martensite structures, $L \approx \rho^{-1/2}$ ranges between 0.03 and 0.1 μm. However, with allowance for the local dislocation clusters (inhomogeneity) we should expect some growth
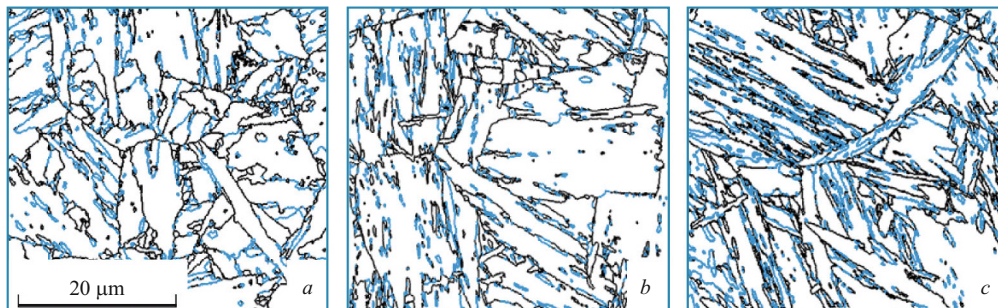
Fig. 6. Boundaries between martensite laths (blue LAB) for the V_2 /V_1 combination of the OR variants against the surrounding in quenched condition (*a*) and after tempering at 660°C for 1 h (*b*) and 6 h (*c*). The black color is used for the rest of the boundaries with misorientations exceeding 5°.
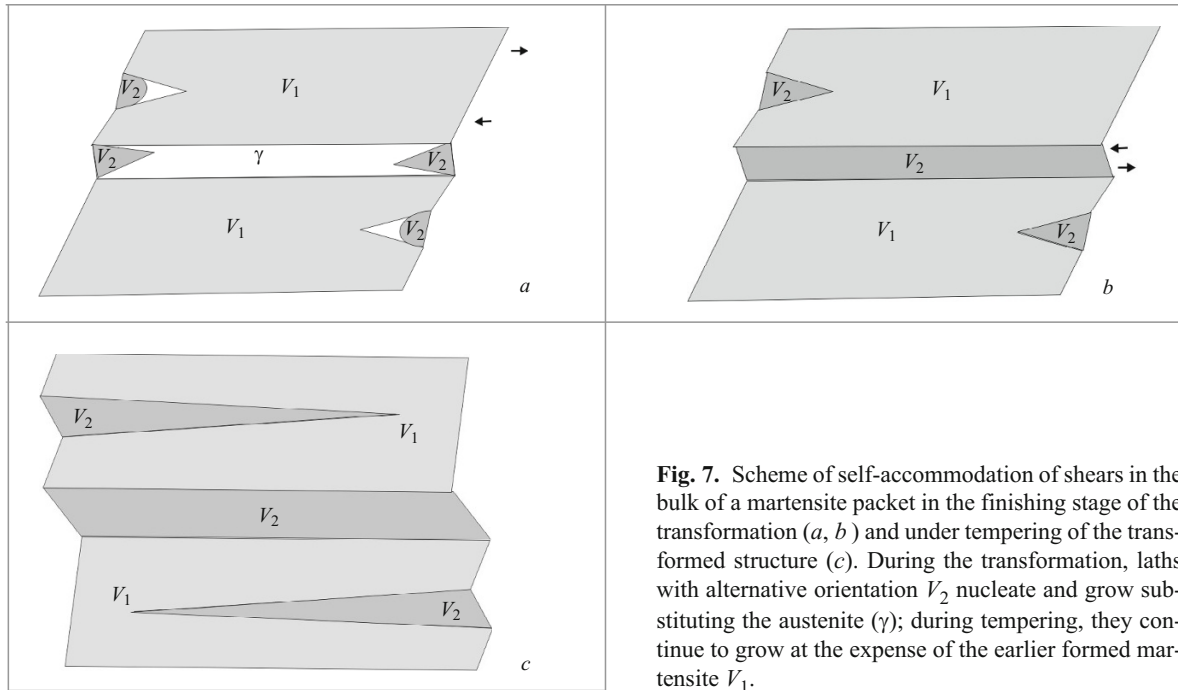
Fig. 7. Scheme of self-accommodation of shears in the bulk of a martensite packet in the finishing stage of the transformation (*a*, *b*) and under tempering of the transformed structure (*c*). During the transformation, laths with alternative orientation V_2 nucleate and grow substituting the austenite (γ); during tempering, they continue to grow at the expense of the earlier formed martensite V_1.

of *L*. Thus, we can hardly predict accurately the relation between ρ and the mapped curvature (the ratio of the GAM to *d*) at a scanning step of 0.1 μm. However, even without pretending to solve the problem, which would require a laborious study with the use of TEM, we may obtain important information on the structural state from the curvature distribution spectra. We have used this approach to analyze the kinetics of tempering of a martensitic steel and determined the difference in its structural components from the rate of its softening.

Variation of the crystal lattice curvature during tempering is quite predictable with allowance for the earlier studies [4 – 9], whereas the growth of individual martensite laths in the transformed structure is a nontrivial effect and requires special discussion. Hypothetically, this effect may be connected with the action of two alternative mechanisms, i.e., (*1*) migration of LAB between the structural components of the α-phase (θ ≈ 60° for V_2/V_1) and (*2*) continuation of the unfinished γ – α transformation in the layers of retained austenite. However, the morphological features (Fig. 6) allow us to exclude the latter alternative. Indeed, in contrast to the retained austenite of the former α-grains or between martensite packets, the layers between adjacent laths, if they exist, are an order of magnitude thinner than the V_2 crystals in Fig. 6. At least, this is so for the studied low-carbon steel 09KhN4MDF.

To understand the driving force of the first of the mechanisms mentioned we should consider the following circumstances.

1. The isolated location and the low volume fraction of the laths in question after quenching (Fig. 6*a*) reflect their formation in the concluding stage of the martensitic transformation, when the phase deformations of whole packets attain maximum values (Fig. 7*a*) and their mutual constraint generates the highest stresses.

2. The orientations of such laths (V_2) and of the packets (V_1) in which they appear and grow belong to different "Bain groups" [10, 11], which means that the difference in the shifts in the corresponding directions is the highest, as it is illustrated by the simplified two-dimensional scheme in Fig. 7*b*. In other words, laths V_2 are the most effective under self-accommodation of the interacting packets, which lowers the internal stresses.

Since such stresses do not disappear after quenching, i.e., the driving force for growth of individual laths V_2 is preserved, such a process may continue under specific kinetic conditions in the absence of retained austenite (Fig. 7*c*), i.e., due to decrease in the fraction of V_1 in the α-phase. During tempering, such conditions (migration mobility of HAB V_2/V_1) are provided by the high enough homological temperature $T/T_m ≈ 0.5$, where T_m is the absolute temperature of melting of the steel. The role of the thermal activation in this process is proved indirectly, for example, by the stronger dependence of the result on the temperature than on the duration of the tempering, which has been mentioned already when we compared Fig. 4*b* and *c*.

The fact that the V_2 crystals that have nucleated in the last stage of the martensitic transformation under the action of internal stresses (Fig. 7*b*) grow under tempering of the transformed structure (Fig. 7*c*) indicates migration of HAB between laths. At the same time, we should mention the specific differences of this process from conventional recrystallization [14], i.e., (*1*) its driving force is determined by the elastic interaction of whole crystalline components of the mi-

cron scale level rather than by the specific energy of the lattice dislocations and (*2*) the propagation of some laths in the α-phase of some laths at their invariable thickness reflects a special "frontal" mechanism of growth like in the cases of thin twins or shear microbands.

Further study of the process considered seems expedient, because refinement of the effective structural components with growth of the specific length of HAB is commonly favorable for the mechanical properties of the material. For the low-carbon steels this acquires a special practical significance because the specific effect of the tempering related to the evolution of the carbide phases is manifested in them relatively weakly.

CONCLUSIONS

We have used steel 09KhN4MDF to test the method of study of the evolution of the structural state of high-strength steels during high tempering with the help of EBSD. The results obtained show that the volume fractions and the spatial distributions of martensite and bainite after quenching are reflected objectively by maps of the crystal lattice curvature, and the rate of softening of different types of α-phase under the tempering may be estimated in terms of the variation of the curvature spectrum. This method has allowed us to detect considerable inhomogeneity of the structure of martensite in quenched steel 09KhN4MDF with respect to the resistance to tempering. In addition to mapping the curvature, processing of EBSD orientation data makes it possible to determine the interphase OR and to analyze the statistics of conjugation of its possible variants on phase boundaries. This approach has allowed us to detect an important tempering effect in the studied steel, i.e., growth of some martensite laths limited by HAB, which lowers the level of the internal stresses due to the self-accommodation of packets and the effective size of the structural components.

REFERENCES

1. B. L. Adams, S. I. Wright, and K. Kunze, "Orientation imaging: The emergence of new microscopy," *Metall. Trans. A*, **24**(4), 819 – 831 (1993).

2. A. J. Wilkinson, G. Meaden, and D. J. Dingley, "High-resolution elastic strain measurement from electron backscatter diffraction patterns: New level of sensitivity," *Ultramicroscopy*, **106**, 307 – 313 (2006).

3. S. Sun, B. L. Adams, and W. E. King, "Observation of lattice curvature near the interface of a deformed aluminum bicrystal," *Phil. Mag. A*, **80**, 9 – 25 (2000).

4. A. A. Zisman, S. Van Boxel, M. Seefeldt, and P. Van Houte, "Gradient matrix method to image crystal curvature by processing of EBSD data and trial recognition of low-angle boundaries in IF steel," *Mater. Sci. Eng. A*, **474**, 165 – 172 (2008).

5. Ch. Rehrl, S. Kleber, O. Renk, and R. Pippan, "Effect of grain size in compression deformation on the microstructural evolution of an austenitic stainless steel," *Mater. Sci. Eng. A*, **540**, 55 – 62 (2012).

6. N. Perano, Y. J. F. Roters, and D. Raabe, "Microstructure and texture evolution in dual-phase steels: Competition between recovery, recrystallization and phase transformation," *Mater. Sci. Eng. A*, **527**, 4161 – 4168 (2010).

7. S. I. Wright, M. M. Nowell, and D. P. Field, "A review of strain analysis using electron backscatter diffraction," *Microsc. Microanal.*, **17**, 316 – 329 (2011).

8. R. Petrov, L. Kestens, A. Wasilkowska, and Y. Houbaert, "Microstructure and texture of a lightly deformed TRIP-assisted steel characterized by means of EBSD technique," *Mater. Sci. Eng. A*, **447**, 285 – 297 (2007).

9. A. A. Zisman, S. N. Petrov, and A. V. Ptashnik, "Quantitative certification of bainitic-martensitic structures of high-strength alloy steels by methods of scanning electron microscopy," *Metallurg*, No. 11, 91 – 95 (2014).

10. G. Miyamoto, N. Iwata, N. Takayama, and T. Furuhara," "Quantitative analysis of variant selection in ausformed lath martensite," *Acta Mater.*, **60**, 1139 – 1148 (2012).

11. N. Takayama, G. Miyamoto, and T. Furuhara, "Effects of transformation temperature on variant pairing of bainitic ferrite in low carbon steel," *Acta Mater.*, **60**, 2387 – 2396 (2012).

12. N. Yu. Zolotarevsky, S. N. Panpurin, A. A. Zisman, and S. N. Petrov, "Effect of ausforming and cooling condition on the orientation relationship in martensite and bainite of low carbon steels," *Mater. Charact.*, **107**, 278 – 282 (2015).

13. N. Yu. Zolotarevsky, A. A. Zisman, S. N. Panpurin, et al., "Effect of grain size and deformation substructure on crystallographic features of bainite and martensite of low-carbon steels," *Metalloved. Term. Obrab. Met.*, No. 10(700), 39 – 48 (2013).

14. T. Tsuchiyama, M. Natori, N. Nakada, and S. Takaki, "Conditions for grain boundary bulging during tempering of lath martensite in ultra-low carbon steel," *ISIJ Int.*, **50**(5), 771 – 773 (2010).